PHYSICAL REVIEW B VOLUME 50, NUMBER 14 1 OCTOBER 1994-II

Thermal fluctuations and NMR spectra of incommensurate insulators

J. Dolinšek, A. M. Fajdiga-Bulat, T. Apih, and R. Blinc
"Josef Stefan" Institute, 61111 Ljubljana, Jamova 39, Slovenia

D. C. Ailion
Department of Physics, University of Utah, Salt Lake City, Utah 84112

(Received 7 March 1994; revised manuscript received 20 June 1994)

The effects of thermal order-parameter fluctuations on the NMR line shape of incommensurate systems are evaluated within the mean-field Landau theory and the results are compared with the ^{87}Rb and ^{39}K $\frac{1}{2}\rightarrow-\frac{1}{2}$ NMR spectra of Rb_2ZnCl_4 and K_2SeO_4 just below the paraelectric-incommensurate transitions. We show that thermal fluctuations do not only reduce the effective incommensurate splitting as compared to the static case but also change the shape of the spectrum. In particular they remove the δ-function-like form of the two edge singularities in analogy to the Debye-Waller factor in x-ray scattering. Two-dimensional NMR separation techniques allow for a separate observation of static and dynamic incommensurate line shapes close to the paraelectric-incommensurate transition temperature T_I. The static inhomogeneously broadened NMR line shape results from the static distribution of quadrupole-perturbed Zeeman frequencies, reflecting the frozen-out incommensurate modulation wave. The dynamic line shape reflects the time-dependent part of the electric quadrupole interaction resulting from phason and amplitudon thermal fluctuations of the modulation wave. Close to T_I these fluctuations become so low in frequency that they influence the line shape. A precise determination of T_I can be obtained from the maximum in the width of the dynamic line shape.

I. INTRODUCTION

Magnetic resonance techniques have been widely used in the past decade to study the local structure of the incommensurate modulation wave in both dielectrics[1,2] and charge density wave systems.[3,4] At the normal-incommensurate (N-I) phase transition T_I the NMR line becomes inhomogeneously broadened.[1] In the incommensurate phase it acquires a specific form[1] showing singularities at the edges. This reflects the spatial variation of the NMR or nuclear quadrupole resonance (NQR) frequencies due to the formation of the incommensurate modulation wave and the breaking of the translational periodicity of the crystal. The width of the incommensurate frequency distribution is in the simplest case directly proportional to the amplitude of the modulation wave and thus reflects the temperature variation of the incommensurate order parameter. Close to T_I thermal fluctuations modify the shape of the NMR line.[5–7] An approximate theory of the NMR line shape, appropriate for fast thermal phase fluctuations and a stationary Gaussian distribution of local phases, has been developed.[5] This theory predicts a motional narrowing of the NMR line close to T_I showing up in a reduced splitting of the edge singularities, but no change in the characteristic incommensurate line shape as T_I is approached from below. The results cannot explain all the complex features observed in NMR, NQR, and electron paramagnetic resonance (EPR) experiments[7–11] close to T_I, which clearly show not only a change in the width of the spectrum, but also a change in the shape of the line.

Here we present a theory of the NMR line shape in incommensurate systems in the presence of thermal fluctuations,[12–16] which is valid within the Landau theory[15,16] and which is capable of describing the transition from the paraelectric to the incommensurate phase. A short account of a part of this theory has been published recently.[12] Here we present a complete description of this theory and extend it to the case where the relation between the NMR frequency and the incommensurate displacements contains also quadratic terms. The theory takes into account both phason and amplitudon fluctuations.[16] It describes the transition from the static incommensurate frequency distribution, which in the absence of thermal fluctuations is limited by two edge singularities, to the motionally averaged single line very close to T_I. To a scaling factor the NMR line shape depends on just two parameters. The theory allows one to specify the conditions for the collapse of the incommensurate broadening. We find that the conditions contain also the dynamic parameters of the crystal. We also show that two-dimensional (2D) NMR provides a unique possibility for a separate simultaneous observation of static and dynamic incommensurate line shapes. The former reflects the static spatial variation of the frozen-in modulation wave, whereas the latter is affected by the time fluctuations of the amplitude and phase of the modulation wave. Those fluctuations are slowed down in the vicinity of the paraelectric-incommensurate transition to the extent that they influence the NMR line shape in a narrow temperature interval around the transition temperature T_I. This in turn allows one to determine precisely T_I in the region where the order-parameter fluctuations are large enough to completely motionally narrow the static incommensu-

rate line shape. The theoretical line shapes are compared with the experimental results for the ^{87}Rb $\frac{1}{2}\rightarrow-\frac{1}{2}$ NMR spectra of Rb_2ZnCl_4 and ^{39}K $\frac{1}{2}\rightarrow-\frac{1}{2}$ spectra of K_2SeO_4 just below the paraelectric-incommensurate transition. A good agreement between theory and experiments is found.

II. ORDER-PARAMETER SPECTRAL DENSITY

We restrict the discussion here to the case of a one-dimensionally modulated incommensurate system with a two-component order parameter,[1,2] i.e., to the case where the soft mode, which induces the *N-I* phase transition, belongs to a two-dimensional representation of the "normal" phase space group at a general point $\mathbf{k}=\mathbf{k}_0$ inside the Brillouin zone.

In the *I* phase we write the nonequilibrium free energy F in the vicinity of T_I as a function of the two-component order parameter ρ_1 and ρ_2 as[1,15,16]

$$F(\rho_1,\rho_2)=\int dV\left\{\frac{\tilde{\alpha}}{2}(\rho_1^2+\rho_2^2)+\frac{\beta}{4}(\rho_1^2+\rho_2^2)^2 -\lambda(\rho_1\nabla\rho_2-\rho_2\nabla\rho_1) +\frac{\delta}{2}[(\nabla\rho_1)^2+(\nabla\rho_2)^2]\right\}, \tag{1a}$$

where $\tilde{\alpha}=\alpha_0(T-T_I)$, $\alpha_0,\beta,\delta,\lambda>0$, and $\nabla=\partial/\partial x$. It is convenient to make a transformation

$$\eta_1=\rho_1\cos k_0x+\rho_2\sin k_0x\ , \qquad \eta_2=-\rho_1\sin k_0x+\rho_2\cos k_0x\ , \tag{1b}$$

with $k_0=\lambda/\delta$, which eliminates the Lifshitz invariant $\lambda(\rho_1\nabla\rho_2-\rho_2\nabla\rho_1)$ from Eq. (1a). We thus obtain

$$F(\eta_1,\eta_2)=\int dV\, g(\eta_1,\eta_2) =\int dV\left\{\frac{\alpha}{2}(\eta_1^2+\eta_2^2)+\frac{\beta}{4}(\eta_1^2+\eta_2^2)^2 +\frac{\delta}{2}[(\nabla\eta_1)^2+(\nabla\eta_2)^2]\right\}, \tag{1c}$$

where $\alpha=\tilde{\alpha}-\delta k_0^2$ and k_0 is the equilibrium wave vector. Minimization of $F(\eta_1,\eta_2)$ with respect to η_1 and η_2 yields the equilibrium solutions

$$\eta_{1E}^2=-\frac{\alpha}{\beta}=A^2\ , \quad \eta_{2E}=0\ , \tag{1d}$$

for the amplitude and the phase of the order parameter.

In the close vicinity of T_I, where the plane-wave approximation is valid, the incommensurate distortion $\eta(x)$ can be expressed as

$$\eta(x)\propto\eta_1\cos k_0x+\eta_2\sin k_0x\ . \tag{2a}$$

Thermal fluctuations will disturb the equilibrium displacements, resulting in a time-dependent η,

$$\eta(x,t)\propto\eta_1(x,t)\cos k_0x+\eta_2(x,t)\sin k_0x\ . \tag{2b}$$

Here $\eta_1(x,t)$ represents the amplitudon and $\eta_2(x,t)$ the phason fluctuations.

We construct the Lagrangian density L by adding to the free-energy density $g(\eta_1,\eta_2)$ the external random driving forces $f_{\eta_{1,2}}$, coupled to the order parameter,

$$f_{\rm ext}=-\eta_1f_{\eta_1}-\eta_2f_{\eta_2}\ , \tag{3}$$

so that

$$L=-g-f_{\rm ext}\ . \tag{4}$$

We assume that the incommensurate modulation wave is overdamped and introduce the dissipation function density[15]

$$R=\frac{\gamma}{2}(\dot{\eta}_1^2+\dot{\eta}_2^2)\ , \tag{5}$$

where the dot stands for the time derivative.

The equations of motion are now obtained from[15]

$$\frac{d}{dx}\frac{\partial L}{\partial\nabla\eta_i}-\frac{\partial L}{\partial\eta_i}=-\frac{\partial R}{\partial\dot{\eta}_i}\ , \quad i=1,2\ . \tag{6}$$

We are interested in small variations of η_1 and η_2 about their equilibrium values, $\eta_1'(x,t)=\eta_1(x,t)-\eta_{1E}$ and $\eta_2'(x,t)=\eta_2(x,t)-\eta_{2E}$. The resulting equations of motion are linearized. The spectral densities of the Fourier components of the amplitudon and phason order-parameter fluctuations

$$\eta_i'(x,t)=\sum_{\omega,q}\eta_i'(\omega,q)e^{i(qx+\omega t)}\ , \quad i=1,2\ ,$$

are obtained in the form

$$\langle|\eta_1'(\omega,q)|^2\rangle=\frac{1}{\pi V}\frac{\gamma k_BT}{\gamma^2\omega^2+(-2\alpha+\delta q^2)^2}\ , \tag{7a}$$

$$\langle|\eta_2'(\omega,q)|^2\rangle=\frac{1}{\pi V}\frac{\gamma k_BT}{\gamma^2\omega^2+\delta^2q^4}\ . \tag{7b}$$

Here V is the crystal volume, $\mathbf{q}=\mathbf{k}-\mathbf{k}_0$, the brackets $\langle\cdots\rangle$ designate a thermodynamic ensemble average, and the identity

$$\langle|f\eta_i(\omega,q)|^2\rangle=\frac{\gamma k_BT}{\pi V} \tag{8}$$

has been used. This identity has been derived[13] for the case that the generalized random forces show no space or time correlations. Since $\eta_1'(x,t)$ and $\eta_2'(x,t)$ are normal excitations of the incommensurate phase they are not correlated:

$$\langle\eta_1'(\omega,q)\eta_2'(-\omega,-q)\rangle=0\ . \tag{9}$$

So far we have assumed that the incommensurate wave is overdamped. Let us now consider the case of an underdamped mode. In that case we have to add to the Lagrangian density [Eq. (4)] a kinetic energy density

$$K=\frac{\mu}{2}(\dot{\eta}_1^2+\dot{\eta}_2^2)\ , \tag{10}$$

so that $L=K-g-f_{\rm ext}$. Here μ is the effective-mass coefficient. Equation (6) has to be replaced by

$$\frac{d}{dt}\frac{\partial L}{\partial \dot{\eta}_i}+\frac{d}{dx}\frac{\partial L}{\partial \nabla \eta_i}-\frac{\partial L}{\partial \eta_i}=-\frac{\partial R}{\partial \dot{\eta}_i}\ , \quad i=1,2\ . \quad (11)$$

In the long-wavelength limit we write the phason and amplitudon dispersion relations for an ideal crystal as

$$\omega_{1q}^2=\nabla_1^2+\kappa q^2\ , \quad (12a)$$

$$\omega_{2q}^2=\kappa q^2\ , \quad (12b)$$

where $\kappa=\delta/\mu$. Both modes are damped with a constant damping factor $\Gamma=\gamma/\mu$. The amplitudon mode has an intrinsic gap $\Delta_1^2=(2\alpha_0/\mu)(T_I-T)$ in the excitation spectrum, whereas the phason gap for an ideal incommensurate phase vanishes. In real systems defects and discrete lattice effects pin the modulation wave and introduce a gap in the phason excitation spectrum[16,18] so that Eq. (12b) becomes

$$\omega_{2q}^2=\Delta_2^2+\kappa q^2\ . \quad (13)$$

The order-parameter spectral densities are now obtained as[1,13]

$$\langle|\eta_i'(\omega,q)|^2\rangle=\frac{\Gamma k_B T}{\pi\mu V[\Gamma^2\omega^2+(\omega^2-\Delta_i^2-\kappa q^2)^2]}\ , \quad i=1,2\ . \quad (14)$$

In the limit $\mu\rightarrow 0$ one recovers the results of an overdamped mode [Eqs. (7a) and (7b)].

III. THE ADIABATIC NMR LINE SHAPE

A. Linear case

The effect of phason and amplitudon fluctuations on the spin-lattice relaxation rate of incommensurate systems has been considered in detail.[1,2] Let us now investigate the effect of these fluctuations on the NMR line shape. We shall assume first that the NMR resonance frequency Ω of a nucleus at a site x is linearly related to the displacement $\eta(x,t)$ at that site:

$$\Omega(x,t)=\Omega_0+a\eta(x,t)\ , \quad (15a)$$

where

$$\eta(x,t)\propto[\eta_{1E}+\eta_1'(x,t)]\cos k_0x+\eta_2'(x,t)\sin k_0x\ . \quad (15b)$$

The adiabatic NMR line shape $I(\omega)$ is now obtained as[14]

$$I(\omega)=\int_0^\infty G(t)e^{i\omega t}dt\ , \quad (16)$$

where the autocorrelation function $G(t)$ is defined as

$$G(t)=e^{-i\Omega_0 t}\langle\langle \exp -i\int_0^t[\Omega(x,t')-\Omega_0]dt'\rangle\rangle_x\ . \quad (17)$$

The inner brackets of the symbol $\langle\langle\cdots\rangle\rangle_x$ represent a thermodynamic ensemble average, whereas the outer brackets $\langle\cdots\rangle_x$ represent the average over the inhomogeneous static distribution function of resonance frequencies. From Eqs. (15a) and (15b) it follows that for the static case $\Omega(x)=\Omega_0+\eta_{1E}\cos k_0x$. We define $X=\cos k_0x$ and find the distribution function $P(X)$ from the identity

$$P(X)dX=n(x)dx=\text{const}\times dx\ ,$$

where $n(x)$ represents a (constant) one-dimensional density of nuclei along the direction of the modulation wave. The average $\langle\cdots\rangle_x$ is thus defined as

$$\langle\cdots\rangle_x\Longrightarrow\int_{-1}^{1}\frac{dX}{\sqrt{1-X^2}}\ .$$

Inserting expression (15b) into (15a), we find the autocorrelation function in the form

$$G(t)=e^{-i\Omega_0 t}\langle\langle G_1(t)G_2(t)\rangle\rangle_x\ , \quad (18a)$$

where

$$G_1(t)=e^{-ia\eta_{1E}t\cos k_0x}\ , \quad (18b)$$

and

$$G_2(t)=\exp -ia\int_0^t[\eta_1'(x,t')\cos k_0x+\eta_2'(x,t')\sin k_0x\,]dt'\ . \quad (18c)$$

We perform the ensemble average first by taking the order-parameter fluctuation probability distribution to be stationary and Gaussian. We use the relation[14]

$$\langle\exp\{-i\int_0^t\omega(t')dt'\}\rangle=\exp\{\langle-\tfrac{1}{2}[\int_0^t\omega(t')dt']^2\rangle\}\ .$$

Taking into account that various Fourier components $\eta_i'(\omega,q)$ of the order-parameter fluctuations

$$\eta_i'(x,t)=\sum_{\omega,q}\eta_i'(\omega,q)e^{i(qx+\omega t)}$$

are statistically independent, we obtain after performing the ensemble average

$$\langle G_2(t)\rangle=\exp\left\{-a^2\left[\sum_{\omega,q}\langle|\eta_1'(\omega,q)|^2\rangle\frac{1-\cos\omega t}{\omega^2}\cos^2k_0x+\sum_{\omega,q}\langle|\eta_2'(\omega,q)|^2\rangle\frac{1-\cos\omega t}{\omega^2}\sin^2k_0x\right]\right\}\ . \quad (19)$$

Next we perform the summation over q. We replace the summation by an integration over half of the Brillouin zone[1,16] between 0 and $|k_{\max}|$:

$$\sum_q\rightarrow\frac{V}{2\pi^2}\int_0^{|k_{\max}|}q^2dq\ .$$

We define

$$\langle|\eta_i'(\omega)|^2\rangle=\frac{V}{2\pi^2}\int_0^{|k_{\max}|}\langle|\eta_i'(\omega,q)|^2\rangle q^2dq\ ,$$

and perform the integration using Eq. (14). We get

$$\langle|\eta_i(\omega)|^2\rangle=\frac{k_BTi}{2\pi^3\mu\kappa^{3/2}\omega}\left\{(\Delta_i^2-\omega^2+i\Gamma\omega)\times\arctan\frac{\kappa^{1/2}k_{\max}}{[\Delta_i^2-\omega^2+i\Gamma\omega]^{1/2}}-\text{c.c.}\right\}. \tag{20}$$

The above expression for the order-parameter spectral density is rather complicated and it is difficult to proceed analytically. The NMR line shape, however, will be affected only by those fluctuations which are slower than the nuclear Larmor frequency, $\omega<\omega_L$, where $\omega_L\approx10^8$ Hz. In the following we will take into account this restriction and treat separately three cases with respect to the size of the gap Δ_i.

(i) *Amplitudon fluctuations* ($\Delta_1=\sqrt{-2\alpha/\mu}$). We take into account that $\kappa^{1/2}q_{\max}=\omega_{\rm ph}$ is of the order of phonon frequencies[13] $\sim10^{13}$ s^{-1}, whereas NMR frequencies fall in the range 10^3-10^8 s^{-1}. Thus we have $\omega_{\rm ph}\gg\omega$. In the range of validity of the mean-field approximation (MFA) theory ($\sqrt{-2\alpha/\delta}=r_C^{-1}\le k_{\max}$), where r_C is the correlation radius for the amplitude of the modulation wave,[2] we also have $\Delta_1\gg\omega,\omega_L$. The damping constant Γ determines the phonon line width and is of the order[11] $(10^{-2}-10^0)\omega_{\rm ph}$. Expression (20) now simplifies to

$$\langle|\eta_1'(\omega)|^2\rangle\approx\frac{k_BT\Gamma}{8\pi^2\mu\kappa^{3/2}\Delta_1},\quad\omega_{\rm ph}>\Delta_1\gg\omega,\sqrt{\Gamma\omega}\ . \tag{21a}$$

(ii) *Phase fluctuations for the case of a large phason gap* ($\Delta_2\gg\omega_L$). We get the same formal expression as in the case of amplitudon fluctuations with the phason gap Δ_2 replacing the amplitudon gap Δ_1:

$$\langle|\eta_2'(\omega)|^2\rangle\approx\frac{k_BT\Gamma}{8\pi^2\mu\kappa^{3/2}\Delta_2},\quad\omega_{\rm ph}>\Delta_2\gg\omega,\sqrt{\Gamma\omega}\ . \tag{21b}$$

(iii) *Phase fluctuations for the case of a gap smaller than the Larmor frequency* ($\Delta_2\ll\omega_L$). Here we get

$$\langle|\eta_2'(\omega)|^2\rangle\approx\frac{k_BT\sqrt{2\Gamma}}{8\pi^2\mu\kappa^{3/2}\sqrt{\omega}},\quad\omega_{\rm ph}>\Gamma\gg\omega\ , \tag{21c}$$

and the fluctuations diverge for $\omega\to0$.

The next step in computing $\langle G_2(t)\rangle$ is to perform the summation over ω. Here we have to distinguish two different cases: the case of a large phason gap ($\Delta_2\gg\omega_L$) and the case of a small phason gap ($\Delta_2\ll\omega_L$).

1. Large phason gap ($\Delta_2\gg\omega_L$)

We insert expressions (21a) and (21b) into Eq. (19) and use

$$\int_0^\infty\frac{1-\cos\omega t}{\omega^2}d\omega=\frac{\pi}{2}t\ ,\quad t>0\ . \tag{22}$$

The dynamic contribution to the autocorrelation function in this case becomes

$$\langle G_2(t)\rangle=\exp\{-(\omega_{\rm loc1}t)\cos^2k_0x-(\omega_{\rm loc2}t)\sin^2k_0x\}\ , \tag{23}$$

where the following definitions have been made:

$$\omega_{\rm loc1}=\frac{a^2k_BT\Gamma}{16\pi\mu^{1/2}\kappa^{3/2}\sqrt{2\alpha_0(T_I-T)}}\propto\frac{T}{\sqrt{T_I-T}}\ , \tag{24a}$$

$$\omega_{\rm loc2}=\frac{a^2k_BT\Gamma}{16\pi\mu\kappa^{3/2}\Delta_2}\propto T\ . \tag{24b}$$

$\omega_{\rm loc1}$ and $\omega_{\rm loc2}$ measure the sizes of amplitude and phase fluctuations in frequency units. We write also $X=\cos k_0x$ and define

$$\Omega_1=a\eta_{1E}\propto\sqrt{T_I-T}\ . \tag{24c}$$

The adiabatic NMR line shape is now given by Eq. (16):

$$I(\omega)=\int_{-1}^{1}\frac{dX}{\sqrt{1-X^2}}\int_0^\infty dt\,e^{i(\omega-\Omega_0)t}\langle G_1(t,X)\rangle\langle G_2(t,X)\rangle=\int_{-1}^{1}\frac{dX}{\sqrt{1-X^2}}\frac{\omega_{\rm loc1}X^2+\omega_{\rm loc2}(1-X^2)}{(\omega_{\rm loc1}X^2+\omega_{\rm loc2}(1-X^2))^2+(\omega-\Omega_0-\Omega_1X)^2}\ . \tag{25}$$

On approaching T_I from below, the amplitude fluctuations critically increase in a narrow temperature range whereas the phase fluctuations practically do not change with temperature. The spectrum [Eq. (25)] depends on two parameters

$$\xi_1=\frac{\omega_{\rm loc1}}{\Omega_1}\propto\frac{T}{T_I-T}$$

and

$$\xi_2=\frac{\omega_{\rm loc2}}{\Omega_1}\propto\frac{T}{(T_I-T)^{1/2}}\ ,$$

which measure the relative sizes of fluctuating order-parameter components with respect to the static order parameter itself.

2. Small phason gap ($\Delta_2\ll\omega_L$)

Here we insert expressions (21a) and (21c) into Eq. (19) and use the identity

$$\int_0^\infty\frac{1-\cos\omega t}{\omega^{5/2}}d\omega=\frac{\sqrt{2\pi}}{12}t^{3/2}\ ,\quad t>0\ . \tag{26}$$

The dynamic contribution to the autocorrelation function becomes

$$\langle G_2(t)\rangle = \exp\{-(\omega_{\mathrm{loc1}}t)\cos^2 k_0 x - (\tilde{\omega}_{\mathrm{loc2}}t)^{3/2}\sin^2 k_0 x\}\ , \tag{27a}$$

where ω_{loc1} is given by Eq. (24a) and $\tilde{\omega}_{\mathrm{loc2}}$ is defined as

$$\tilde{\omega}_{\mathrm{loc2}} = \left[\frac{a^2 k_B T \gamma^{1/2}}{48\pi^{3/2}\delta^{3/2}}\right]^{2/3} \propto T^{2/3}\ . \tag{27b}$$

The adiabatic NMR line shape is given by

$$I(\omega) = -\int_{-1}^{1}\frac{dX}{\sqrt{1-X^2}} \times \int_0^\infty dt\, e^{i(\omega-\Omega_0-\Omega_1 X)t} \times e^{-[\omega_{\mathrm{loc1}}tX^2+(\tilde{\omega}_{\mathrm{loc2}}t)^{3/2}(1-X^2)]}\ . \tag{28}$$

The expression (28) cannot be evaluated analytically because of the $t^{3/2}$ term. Up to a scaling factor it depends on two parameters

$$\xi_1 = \frac{\omega_{\mathrm{loc1}}}{\Omega_1} \propto \frac{T}{T_I - T}$$

and

$$\tilde{\xi}_2 = \frac{\tilde{\omega}_{\mathrm{loc2}}}{\Omega_1} \propto \frac{T^{2/3}}{(T_I-T)^{1/2}}\ ,$$

which as before measure the relative sizes of fluctuating and static parts of the order parameter.

A decrease of the parameters ξ_1, ξ_2, and $\tilde{\xi}_2$ corresponds to moving away from the *N-I* phase transition temperature T_I into the incommensurate phase. Far away from T_I, ξ_1, ξ_2, and $\tilde{\xi}_2$ tend to zero and $\langle G_2\rangle \approx 1$. Equations (25) and (28) yield in that case a static incommensurate frequency distribution function,[1] which exhibits two edge singularities at $\pm\Omega_1$,

$$I(\omega) = \frac{1}{\sqrt{1-[(\omega-\Omega_0)/\Omega_1]^2}}\ . \tag{29}$$

Phason and amplitudon fluctuations become important for the NMR line shape in the close vicinity of T_I. According to the Fourier theorem, the product of two functions in the time domain is equivalent to the convolution of their Fourier transforms in the frequency domain. The Fourier transform of $\langle G_2\rangle$ thus represents the dynamic line shape, which convolutes the static line shape Eq. (29).

B. Quadratic case

Let us now look into the case where the NMR frequency Ω of a nucleus at a site x is quadratically related to the displacement $\eta(x,t)$ at this site:

$$\Omega(x,t) = \Omega_0 + b\eta^2(x,t)\ . \tag{30}$$

Here we have as before

$$\eta(x,t) = [\eta_{1E} + \eta_1'(x,t)]\cos k_0 x + \eta_2'(x,t)\sin k_0 x\ ,$$

so that

$$\eta^2(x,t) = \eta_{1E}^2\cos^2 k_0 x + 2\eta_{1E}\eta_1'(x,t)\cos^2 k_0 x + 2\eta_{1E}\eta_2'(x,t)\sin k_0 x\cos k_0 x\ . \tag{31}$$

Terms quadratic in $\eta_1'(x,t)$ and $\eta_2'(x,t)$ have been neglected here. Again we have

$$G(t) = e^{-i\Omega_0 t}\langle\langle G_1(t)G_2(t)\rangle\rangle_x\ , \tag{32a}$$

where now

$$G_1(t) = e^{-ib\eta_{1E}^2\cos^2(k_0x)t} \tag{32b}$$

and

$$G_2(t) = \exp -i\tilde{b}\int_0^t [\eta_1'(x,t')\cos^2(k_0x) + \eta_2'(x,t')\sin(k_0x)\times\cos(k_0x)]dt'\ , \tag{32c}$$

with

$$\tilde{b} = 2b\eta_{1E}\ . \tag{32d}$$

Expanding $\eta_1'(x,t)$ and $\eta_2'(x,t)$ in a Fourier series in q and ω, and using the same procedure as in the previous section we find for the case of a small phason gap

$$\langle G_2(t)\rangle = \exp -\{(\omega_{\mathrm{loc1}}'t)\cos^4 k_0 x + (\tilde{\omega}_{\mathrm{loc2}}'t)^{3/2}\cos^2 k_0 x\,\sin^2 k_0 x\} \tag{33}$$

with $\omega_{\mathrm{loc1}}' = [\tilde{b}/a]^2\omega_{\mathrm{loc1}}$ and $\tilde{\omega}_{\mathrm{loc2}}' = [\tilde{b}/a]^{4/3}\tilde{\omega}_{\mathrm{loc2}}$.

Introducing

$$X^2 = \cos^2(k_0x) = \frac{\Omega(x)-\Omega_0}{\Omega_2}\ , \tag{34}$$

where $\Omega_2 = b\eta_{1E}^2$, and using $P(X)dX = \mathrm{const}\times dx$ we can again evaluate the spatial average $\langle\cdots\rangle_x$ as

$$\langle\cdots\rangle_x = \int_{-1}^{+1}\frac{dX}{\sqrt{1-X^2}}\ ,$$

so that the adiabatic NMR line shape now becomes

$$I(\omega) = \int_{-1}^{+1}\frac{dX}{\sqrt{1-X^2}}\int_0^\infty dt\, e^{i(\omega-\Omega_0)t}\langle G_1(t)\rangle\langle G_2(t)\rangle$$

$$= \int_{-1}^{+1}\frac{dX}{\sqrt{1-X^2}}\int_0^\infty dt\, e^{i(\omega-\Omega_0-\Omega_2X^2)t}\, e^{-[(\omega_{\mathrm{loc1}}'t)X^4+(\tilde{\omega}_{\mathrm{loc2}}'t)^{3/2}X^2(1-X^2)]}\ . \tag{35}$$

Far away from T_I, $\langle G_2 \rangle \approx 1$ and we recover the static frequency distribution for the quadratic case:

$$I(\omega)=\frac{\text{const}}{\sqrt{[(\Omega_0+\Omega_2-\omega)/\Omega_2][(\omega-\Omega_0)/\Omega_2]}} . \quad (36)$$

The case with a large phason gap is analogous except for the replacement of the $t^{3/2}$ term with a term linear in t. In reality one expects that the expansion of the NMR frequency in powers of the displacements contains both linear and quadratic terms. The expansion of the above theory to this case is trivial.

IV. 2D NMR SEPARATION OF STATIC AND DYNAMIC LINE SHAPES

It is interesting to note that two-dimensional NMR provides for a unique possibility to separate the static inhomogeneous line shape, represented by $\langle G_1 \rangle$, and the dynamic homogeneous line shape, represented by $\langle G_2 \rangle$. The shape of the incommensurate NMR spectrum of a nucleus with spin $I > \frac{1}{2}$ is determined by the electric quadrupole interaction with the electric field gradient (EFG) tensor at the nuclear site. This interaction is space and time modulated by the presence of the incommensurate wave. The static inhomogeneously broadened NMR line shape results from the static distribution of quadrupole-perturbed Zeeman frequencies, reflecting the frozen-out incommensurate modulation wave. Thus it shows directly the static incommensurate distortions. The dynamic line shape, on the other hand, reflects the time-dependent part of the electric quadrupole interaction due to phason and amplitudon fluctuations of the modulation wave. It has been shown[17] that the static quadrupole interaction can be eliminated from one frequency domain in a 2D "separation of interactions" type of NMR experiment (Fig. 1). The 2D line shape shows in the ω_2 frequency domain the normal 1D line shape of Eqs. (25) and (28), which is a convolution of the static line shape with the dynamic one. In the ω_1 domain only the dynamic line shape appears. This is so as the spin precession under the static quadrupole interaction in the first half of the evolution period has been compensated by the opposite precession in the second half of that period. This is achieved by the application of a refocusing pulse in the middle of the evolution period. It is important to note that only the precession under the static quadrupole Hamiltonian can be refocused, whereas the evolution of the spin system under the time-dependent randomly fluctuating quadrupole Hamiltonian cannot be time reversed. The time-dependent part of the Hamiltonian determines the adiabatic line shape and produces relaxation. The term "dynamic line shape" stands here for the adiabatic (homogeneous) line shape and is appropriate when the phason- and amplitudon-induced fluctuations of the EFG tensor slow down to the extent that they influence the line shape. This is the case in the close vicinity of the paraelectric-incommensurate transition temperature T_I.

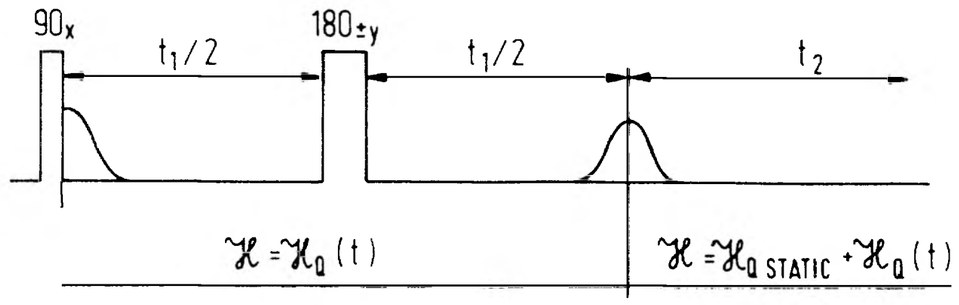

FIG. 1. 2D NMR pulse sequence for elimination of the static part of the quadrupole interaction from the ω_1 domain, while retaining the dynamic part. The sequence is designed for half-integer spins $I > \frac{1}{2}$ with only the central transition $\frac{1}{2} \rightarrow -\frac{1}{2}$ irradiated. Since only two levels are involved the problem is formally equivalent to the separation of chemical shift from dipole coupling for spins $I=\frac{1}{2}$. In the ω_2 domain the static line shape convoluted with the dynamic one is obtained, reflecting the full Hamiltonian $\mathcal{H}_{Q\text{static}}+\mathcal{H}_Q(t)$. In the ω_1 domain, only the dynamic line shape appears, reflecting the dynamic part of the quadrupole Hamiltonian $\mathcal{H}_Q(t)$.

We write the 2D line shape for an incommensurate modulation wave with a large phason gap ($\Delta_2 \gg \omega_L$) in the linear case [Eq. (15a)] in the form

$$I(\omega_1,\omega_2)=\int_{-1}^{1}\frac{dX}{\sqrt{1-X^2}}\int_0^\infty dt_1\int_0^\infty dt_2 e^{i(\omega_2-\Omega_0-\Omega_1 X)t_2}e^{-t_2[\omega_{\text{loc}1}X^2+\omega_{\text{loc}2}(1-X^2)]}e^{i\omega_1 t_1}e^{-t_1[\omega_{\text{loc}1}X^2+\omega_{\text{loc}2}(1-X^2)]} . \quad (37a)$$

Here t_1 is the evolution and t_2 the detection time of the 2D experiment. The Fourier transform integrals in Eq. (37a) can be done analytically, yielding Lorentzian shapes in both frequency domains:

$$I(\omega_1,\omega_2)=\int_{-1}^{1}\frac{dX}{\sqrt{1-X^2}}\frac{\omega_{\text{loc}1}X^2+\omega_{\text{loc}2}(1-X^2)}{[\omega_{\text{loc}1}X^2+\omega_{\text{loc}2}(1-X^2)]^2+(\omega_2-\Omega_0-\Omega_1X)^2}\frac{\omega_{\text{loc}1}X^2+\omega_{\text{loc}2}(1-X^2)}{[\omega_{\text{loc}1}X^2+\omega_{\text{loc}2}(1-X^2)]^2+\omega_1^2} . \quad (37b)$$

In Eq. (37a) the information on the static distribution of resonance frequencies is retained in the ω_2 domain via the term $e^{i(\omega_2-\Omega_0-\Omega_1X)t_2}$. In the ω_1 domain this information is eliminated by the refocusing effect of the pulse in the middle of the evolution period. The static inhomogeneous line shape convoluted with the dynamic one is obtained as the $\omega_1=0$ cross section of the 2D spectrum [Eq. (37b)]. The dynamic line shape is obtained in the ω_1 domain and varies over the inhomogeneous line shape through its dependence on $X=\cos k_0 x=(\omega_2-\Omega_0)/\Omega_1$.

The theoretical inhomogeneous and dynamic line shapes in the vicinity of T_I are shown in Figs. 2(a) and 2(b). Figure 2(a) shows the inhomogeneous line shape convoluted with the dynamic one as it appears in the ω_2

domain of the 2D NMR experiment. The parameter $\xi_1=\omega_{\mathrm{loc}1}/\Omega_1$ has been varied between 0.5 (closest to T_I) and 0.05 (far away from T_I) reflecting the $T/(T_I-T)$ dependence. The parameter $\xi_2=\omega_{\mathrm{loc}2}/\Omega_1$ has been kept constant for the top five line shapes at a value 0.2 due to a weaker temperature dependence as compared to ξ_1. The line shape at the bottom was obtained with $\xi_2=0.05$ and represents the almost static case. As can be seen, the line shape is drastically changed in the region where the thermal fluctuations are large, whereas outside that region the static incommensurate line shape appears unaffected.

The dynamic line shape is shown in Fig. 2(b) for different values of the parameter ξ_1 between 0.83 and 0.05. The parameter ξ_2 has been fixed at a value 0.2 for the top five line shapes. The line shape at the bottom is obtained with $\xi_2=0.05$, representing the almost static case. The line shape shown is the $\omega_2=\Omega_0$ cross section of the 2D spectrum [Eq. (37b)]. The linewidth exhibits a maximum at $T=T_I$ due to its dependence on $\omega_{\mathrm{loc}1}\propto T/\sqrt{T_I-T}$ and narrows on going away from T_I. As long as the width of the dynamic line shape is comparable to that of the static inhomogeneous line shape, thermal fluctuations drastically affect the shape of the spectrum. Moving away from T_I the dynamic line shape narrows and the static inhomogeneous line shape broadens, so that thermal fluctuations are of increasingly smaller importance.

In the case of a gapless phason ($\Delta_2\ll\omega_L$) the situation is quite different. There the 2D spectrum can be written in the form

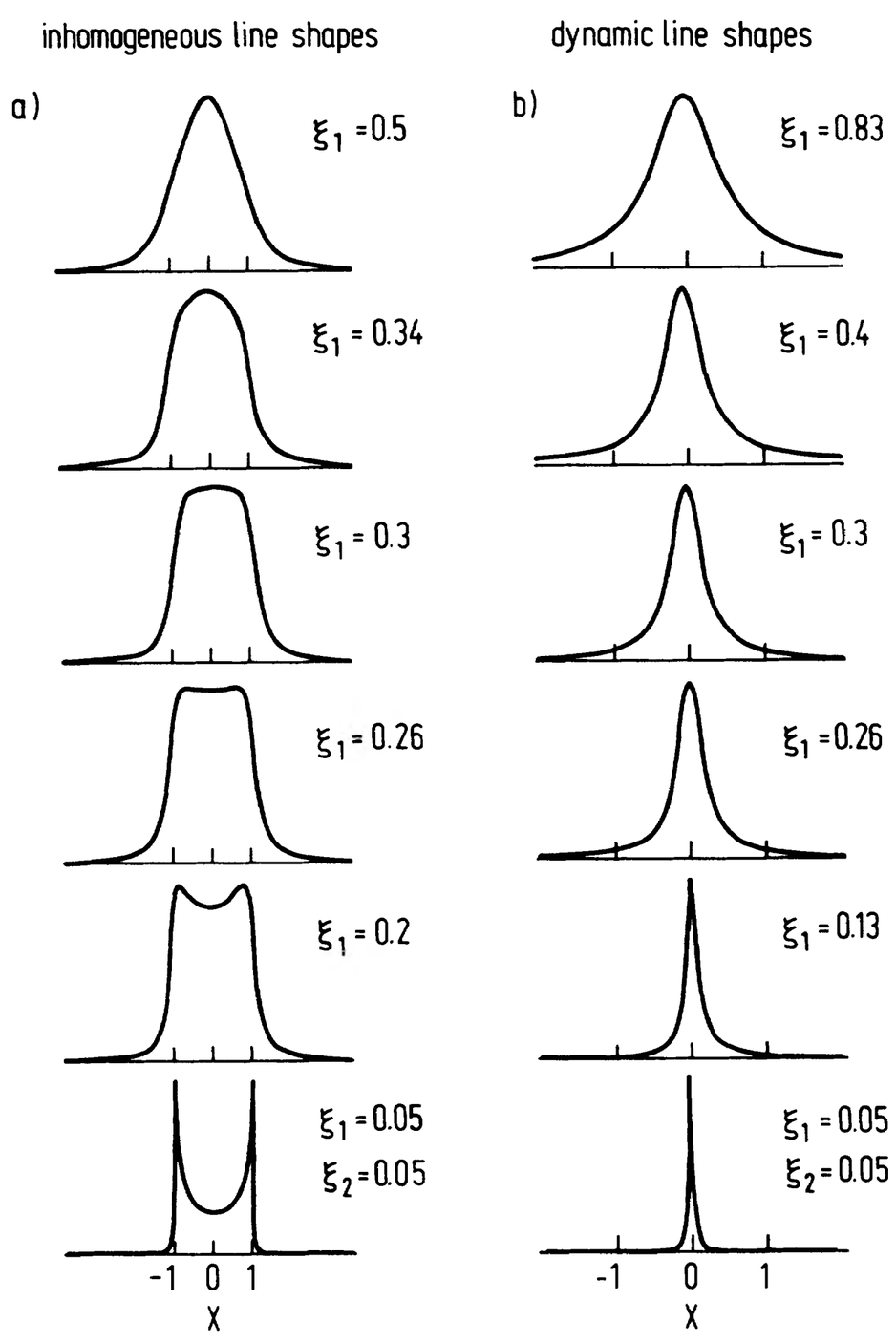

FIG. 2. Linear case. (a) Theoretical static inhomogeneous line shapes convoluted with the dynamic ones in the vicinity of T_I for the case of a phason gap larger than the nuclear Larmor frequency, $\Delta_2\gg\omega_L$. The line shapes are displayed on a normalized frequency scale $X=(\omega-\Omega_0)/\Omega_1$. The parameter $\xi_1=\omega_{\mathrm{loc}1}/\Omega_1$ is varied between 0.5 (closest to T_I) and 0.05 (far away from T_I) while the parameter ξ_2 is kept constant at the value 0.2 for the top five line shapes. The line shape at the bottom represents the almost static case obtained with $\xi_2=0.05$. (b) Theoretical dynamic line shapes for the case of a large phason gap ($\Delta_2\gg\omega_L$). ξ_1 is varied between 0.83 and 0.05. The parameter ξ_2 has a fixed value of 0.2 for the top five line shapes. The line shape at the bottom represents the almost static case obtained with $\xi_2=0.05$.

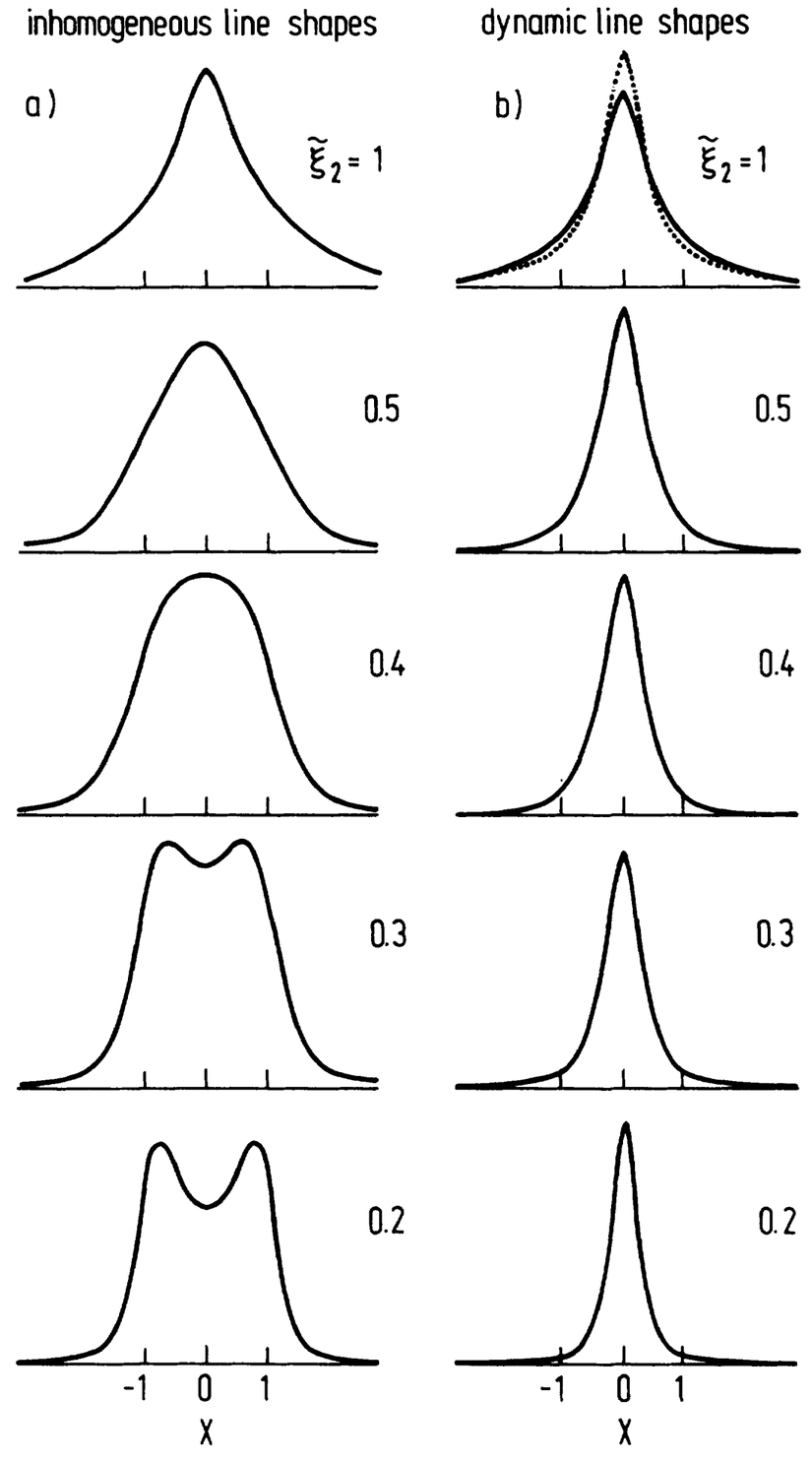

FIG. 3. Linear case. (a) Theoretical static inhomogeneous line shapes convoluted with the dynamic ones in the vicinity of T_I for the case of a small phason gap ($\Delta_2\ll\omega_L$). The line shapes are displayed on a normalized frequency scale $X=(\omega-\Omega_0)/\Omega_1$. The parameter $\tilde{\xi}_2$ is varied between 1 (closest to T_I) and 0.2, whereas ξ_1 has a fixed value of 0.2. (b) Theoretical dynamic line shapes for the case of a small phason gap ($\Delta_2\ll\omega_L$). $\tilde{\xi}_2$ is varied between 1 and 0.2 and $\xi_1=0.2$. A Lorentzian shape (dotted line) is shown for comparison at the top spectrum, where the two lines are scaled to have the same area.

$$I(\omega_1,\omega_2)=\int_{-1}^{1}\frac{dX}{\sqrt{1-X^2}}\int_0^\infty dt_1\int_0^\infty dt_2 e^{i(\omega_2-\Omega_0-\Omega_1X)t_2}e^{-[\omega_{\mathrm{loc}1}t_2X^2+(\tilde{\omega}_{\mathrm{loc}2}t_2)^{3/2}(1-X^2)]}\times e^{i\omega_1t_1}e^{-[\omega_{\mathrm{loc}1}t_1X^2-(\omega_{\mathrm{loc}2}t_1)^{3/2}(1-X^2)]}\quad(38)$$

The Fourier integrals cannot be done analytically due to the $t^{3/2}$ dependence and the corresponding dynamic line shape is no longer Lorentzian. The spectrum depends on two parameters. $\xi_1=\omega_{\mathrm{loc}1}/\Omega_1\propto T/(T_I-T)$ represents as before amplitudon fluctuations, whereas the gapless phason fluctuations are represented by the parameter

$$\tilde{\xi}_2=\frac{\tilde{\omega}_{\mathrm{loc}2}}{\Omega_1}\propto\frac{T^{2/3}}{(T_I-T)^{1/2}}\ .$$

Figure 3(a) shows a set of inhomogeneous NMR spectra, where the parameter ξ_2 has been varied in the range between 1 and 0.2. The parameter ξ_1 has been kept constant at the value 0.2. It can be seen that the line shape with $\tilde{\xi}_2=1$ (closest to T_I) shows a characteristic shape due to the $t^{3/2}$ term. The static inhomogeneous frequency distribution function is here much narrower than the dynamic line shape induced by phase fluctuations. This shape evidently differs from the Lorentzian shape predicted for a phason with a gap. On moving away from T_I ($\tilde{\xi}_2\rightarrow 0$) the line shape transforms into the static line shape. Thermal phase fluctuations are again important only in the close vicinity of T_I, where the dynamic line shape is of comparable width to the static frequency distribution. All spectra are $\omega_1=0$ cross sections of the 2D spectrum [Eq. (38)].

The dynamic line shape for the case of a gapless phason is shown in Fig. 3(b). $\tilde{\xi}_2$ is varied between 1 and 0.2 and ξ_1 is kept constant at 0.2. On the top spectrum a comparison to a Lorentzian shape (dotted line) is made where the two lines have been normalized to have the same area. Due to its $t^{3/2}$ dependence, the dynamic line shape for the case of a gapless phason is narrower in the center and has stronger wings than the Lorentzian line shape. One should thus be able to discriminate between these two possibilities by making precise measurements of the inhomogeneous and dynamic line shapes using the 2D NMR separation of interactions technique.

The 2D line shape for the quadratic case [Eq. (30)] can be treated in the same way using Eq. (35) for $I(\omega)$. In the case of a small phason gap ($\Delta_2\ll\omega_L$) we obtain

$$I(\omega_1,\omega_2)=\int_{-1}^{1}\frac{dX}{\sqrt{1-X^2}}\int_0^\infty dt_1\int_0^\infty dt_2 e^{i(\omega_2-\Omega_0-\Omega_2X^2)t_2}e^{-[\omega'_{\mathrm{loc}1}t_2X^4+(\tilde{\omega}'_{\mathrm{loc}2}t_2)^{3/2}X^2(1-X^2)]}\times e^{i\omega_1t_1}e^{-[\omega'_{\mathrm{loc}1}t_1X^4+(\tilde{\omega}'_{\mathrm{loc}2}t_1)^{3/2}X^2(1-X^2)]}\quad(39)$$

Theoretical spectra close to T_I are shown in Fig. 4. Figure 4(a) shows the inhomogeneous line shapes obtained as the $\omega_1=0$ cross sections of the 2D spectrum [Eq. (39)]. The parameter $\xi'_1=\omega'_{\mathrm{loc}1}/\Omega_2$ has been varied between 0.8 (close to T_I) and 0.1 (far away from T_I), whereas $\xi'_2=\tilde{\omega}'_{\mathrm{loc}2}/\Omega_2$ has been kept constant at a value of 0.8. The line shapes are displayed on a normalized frequency scale $(\omega-\Omega_0)/\Omega_2$. The line shape for $\xi'_1=0.1$ practically corresponds to the static case of Eq. (36), which exhibits two edge singularities of unequal intensities, the larger being centered at $\omega=\Omega_0$. As in the linear case, thermal fluctuations destroy the static shape close to T_I. Figure 4(b) shows the dynamic line shapes obtained as the $\omega_2=0$ cross sections of the 2D spectrum [Eq. (39)]. The parameter ξ'_1 has again been varied between 0.8 and 0.1 and $\xi'_2=0.8$ has been used. As in the linear case, a change in the linewidth is observed.

V. RESULTS AND DISCUSSION

A. ^{87}Rb NMR in Rb_2ZnCl_4

A 2D separation of interactions experiment has been performed on the ^{87}Rb $\frac{1}{2}\rightarrow-\frac{1}{2}$ transition in an ultrapure Rb_2ZnCl_4 crystal at an orientation $a\perp H_0$, $<c,H_0=122°$. At this particular orientation there are two ^{87}Rb lines, originating from the two physically nonequivalent Rb sites of the paraelectric unit cell. The 2D spectrum in the incommensurate phase at $T=291.2$ K is displayed in Fig. 5. In the ω_2 domain the two lines show typical incommensurate shapes with continuous frequency distribution limited by edge singularities—shown in the projection above the 2D spectrum. The domain is sensitive to both the static and the dynamic parts of the quadrupole interaction. Since, however, the spectrum has been taken far below the paraelectric-incommensurate transition, the dynamic parts of the quadrupole interaction has a negligible effect on the line shape. The line shapes in the ω_2 domain are thus here purely static. The effect of phase and amplitude fluctuations on the NMR line shape in the vicinity of T_I has been studied on the left line (centered around $\omega_2/2\pi=0$ Hz). In the ω_1 domain, the static quadrupole interaction is eliminated from the spectrum, which is determined by the dynamic quadrupole interaction and the much weaker magnetic dipole interaction between ^{87}Rb nuclei. At the above orientation the expansion of the resonance frequency in powers of displacements [Eq. (15a)] is well described by the linear term only.[18]

A line-shape study in temperature steps of 0.2 K has been performed in the vicinity of the paraelectric-incommensurate transition. The positions ν_{inh} of the edge singularities obtained in the ω_2 domain are shown in

Fig. 6. The full width at half height of the dynamic line shape $\Delta\nu_H$ obtained in the ω_1 domain at the center of the static line shape is also shown. On the same plot the spin-lattice relaxation time T_1 is also displayed. In the incommensurate phase T_1 varies over the inhomogeneous line shape with $X=\cos k_0 x=(\omega_2-\Omega_0)/\Omega_1$. It has been shown[19,21,22] that the variation is well described by the expression

$$\frac{1}{T_1}=X^2\frac{1}{T_{1A}}+(1-X^2)\frac{1}{T_{1\varphi}}\ , \tag{40}$$

where T_{1A}^{-1} represents the amplitudon-induced and $T_{1\varphi}^{-1}$ the phason-induced spin-lattice relaxation rate. T_{1A} and $T_{1\varphi}$ can thus be separately determined by measuring the spin-lattice relaxation time over the inhomogeneous line

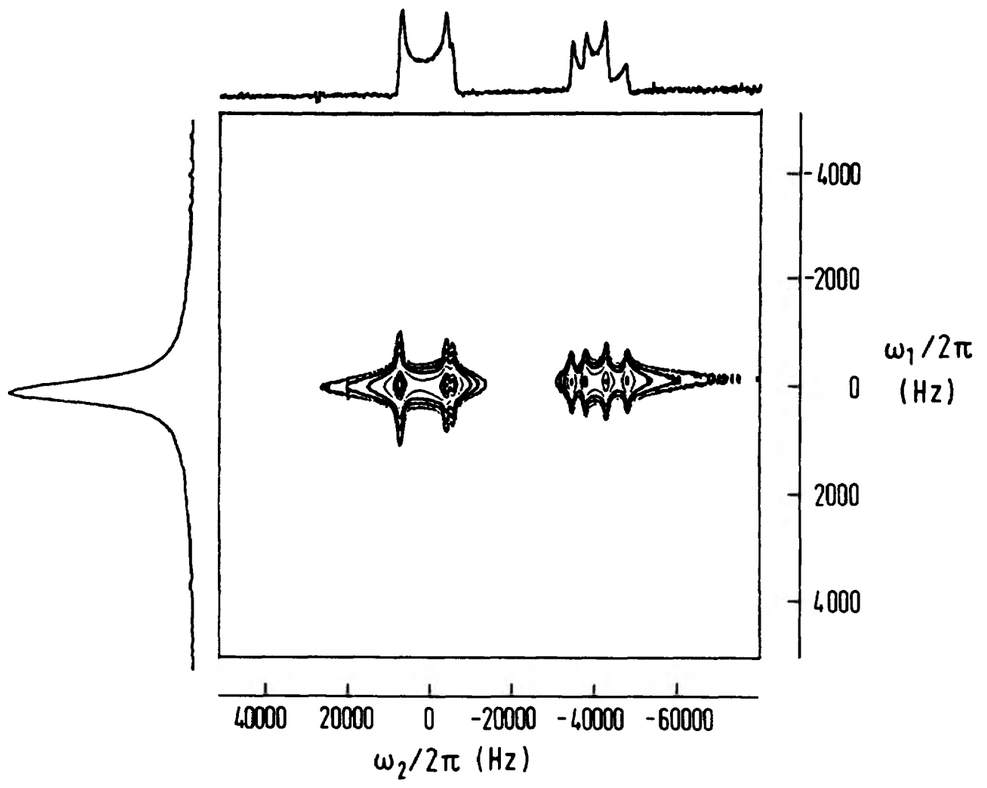

FIG. 5. Two-dimensional separation of interactions magnitude spectrum of the ^{87}Rb $\frac{1}{2}\rightarrow-\frac{1}{2}$ transition in Rb_2ZnCl_4 at an orientation $a\perp H_0$, $<c,H_0=122°$, $T=291.2$ K, and $\nu_0(^{87}\text{Rb})=88.34$ MHz. The ω_2 domain shows the inhomogeneously broadened incommensurate line shape, reflecting the static and dynamic parts of the quadrupole interaction. The ω_1 domain shows the homogeneous line shape, determined by the dynamic part of the quadrupole interaction and the magnetic dipole interaction of ^{87}Rb nuclei. Projections on both frequency axes are also shown. The spectrum is displayed in the magnitude mode.

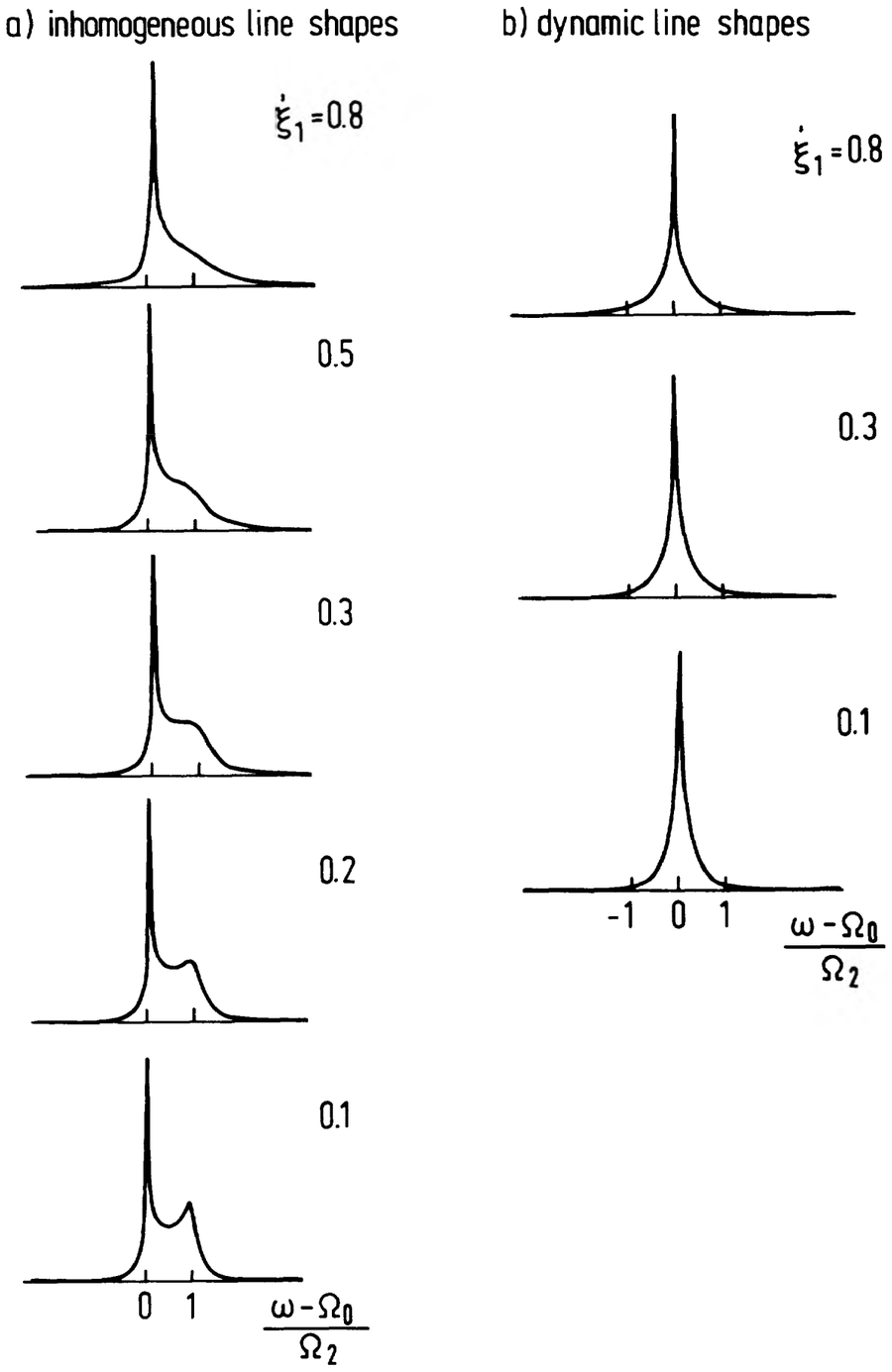

FIG. 4. Quadratic case. (a) Inhomogeneous line shapes close to T_I for the case of a small phason gap ($\Delta_2\ll\omega_L$). Line shapes are the $\omega_1=0$ cross sections of the 2D spectrum [Eq. (39)]. The parameter $\xi_1'=\omega_{\text{loc1}}'/\Omega_2$ has been varied between 0.8 (close to T_I) and 0.1 (far away from T_I), whereas $\xi_2'=\omega_{\text{loc2}}'/\Omega_2$ has been kept constant at a value 0.8. The line shapes are displayed on a normalized frequency scale $(\omega-\Omega_0)/\Omega_2$. Thermal fluctuations close to T_I destroy the static line shape. (b) Dynamic (homogeneous) line shapes close to T_I for the quadratic case and small phason gap ($\Delta_2\ll\omega_L$). Line shapes are the $\omega_2=0$ cross sections of the 2D spectrum [Eq. (39)]. The parameter ξ_1' is varied between 0.8 (close to T_I) and 0.1 (far away from T_I). A fixed $\xi_2'=0.8$ has been used. As in the linear case, the linewidth changes with temperature.

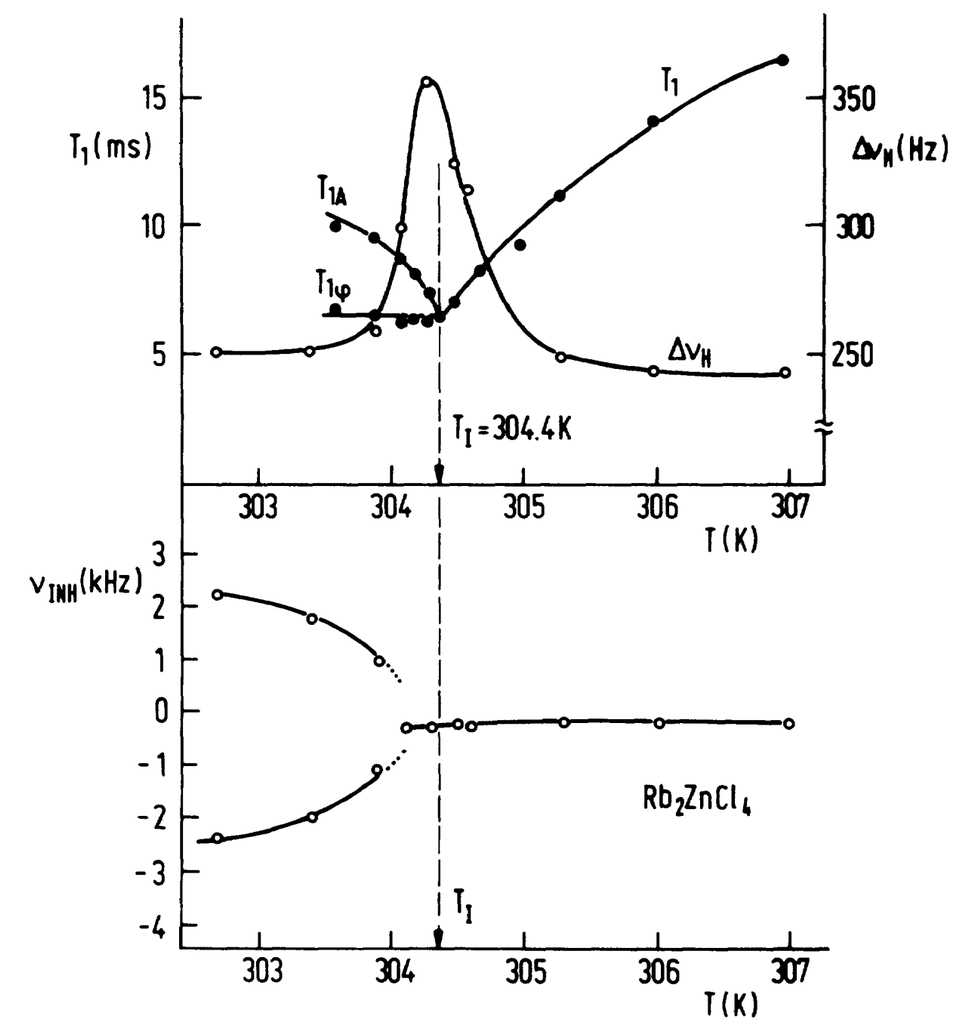

FIG. 6. Temperature dependence of the spin-lattice relaxation time T_1, the full width at half height of the dynamic line shape $\Delta\nu_H$, and the frequencies of edge singularities of the inhomogeneous line shape ν_{inh} in Rb_2ZnCl_4 in a narrow temperature interval around T_I. T_{1A} is the amplitudon- and $T_{1\phi}$ the phason-induced spin-lattice relaxation times. $\nu_0(^{87}\text{Rb})=88.34$ MHz, $a\perp H_0$, $<c,H_0=122°$.

shape. From Fig. 6 it is seen that the width of the dynamic line shape $\Delta\nu_H$ exhibits a maximum at $T_I=304.4$ K. T_1 in the paraelectric phase decreases on lowering the temperature and a minimum value is obtained at T_I. Below T_I, T_1 splits into two branches: the temperature-independent phason contribution $T_{1\varphi}$ and the critically temperature-dependent amplitudon contribution $T_{1A}\propto\sqrt{T_I-T}$. The experimental variation of T_1 over the inhomogeneous line is shown in Fig. 7 for $T_I-T=0.1$ and 0.3 K. The temperature $T_I=304.4$ K is obviously the phase transition temperature, where the paraelectric soft mode condenses. In the vicinity of T_I its frequency becomes so low that it affects the NMR line shape. Thus a very accurate determination of the transition temperature T_I can be made. The inhomogeneous line shape, on the other hand, shows at $T_I=304.4$ K no typical incommensurate shape, limited by two edge singularities. It rather retains its paraelectric shape and starts to broaden with decreasing temperature. The incommensurate splitting starts to be seen at $T_I-T=0.4$ K. The maximum in the dynamic linewidth and the appearance of resolved phason and amplitudon relaxation rates occur at the same temperature, which is different from the temperature where one starts to observe the incommensurate splitting of the inhomogeneous line shape. It is obvious that there exists a critical region below T_I—as determined from the dynamic-line-shape maximum—where the phase and amplitude fluctuations affect the inhomogeneous line shape and destroy its static incommensurate shape. The width of this region is here about 0.4 K. The experimental and theoretical inhomogeneous line shapes close to T_I are shown in Fig. 8(a). At $T_I-T=0.1$ and 0.3 K the inhomogeneous line shape is smeared out by fluctuations so that it exhibits the paraelectriclike shape. At $T_I-T=0.5$ K, a typical incommensurate shape with two edge singularities becomes observable. The theoretical fit represents the $\omega_1=0$ cross section of the 2D spectrum Eq. (37b). The inhomogeneous line shape is not sensitive enough to discriminate between the case of a large [Eq. (37b)] and the case of a small phason gap [Eq. (38)] and both expressions fit the experimental line shape equally well. A discrimination between the two possibilities can be made, however, by comparing the experimental and theoretical dynamic line shapes, which are shown in Fig. 8(b) for the same temperatures. The solid lines represent the fits with Eq. (37b) corresponding to a phason with a large gap whereas the dotted lines represent fits with Eq. (38) valid for a gapless phason. Both fits are $\omega_2=\Omega_0$ cross sections of the 2D spectra where Ω_0 is the position of the absorption line in the paraelectric phase. The fit with a large phason gap reproduces the experimentally observed homogeneous line shapes better than the fit without a phason gap. As can be seen from Fig. 8(b) the difference in the two theoretical fits is not very large. In a good signal-to-noise experimental spectrum it is, however, possible to discriminate between the two cases. The line shape of the gapless-phason case deviates measurably from the Lorentzian form. The evaluation of the phason gap from the line shape is not possible, however. The theory can just discriminate whether the gap is much larger or much smaller than the nuclear Larmor frequency. In Fig. 8(c) the observed inhomogeneous ^{87}Rb line shapes are shown in a larger temperature interval.

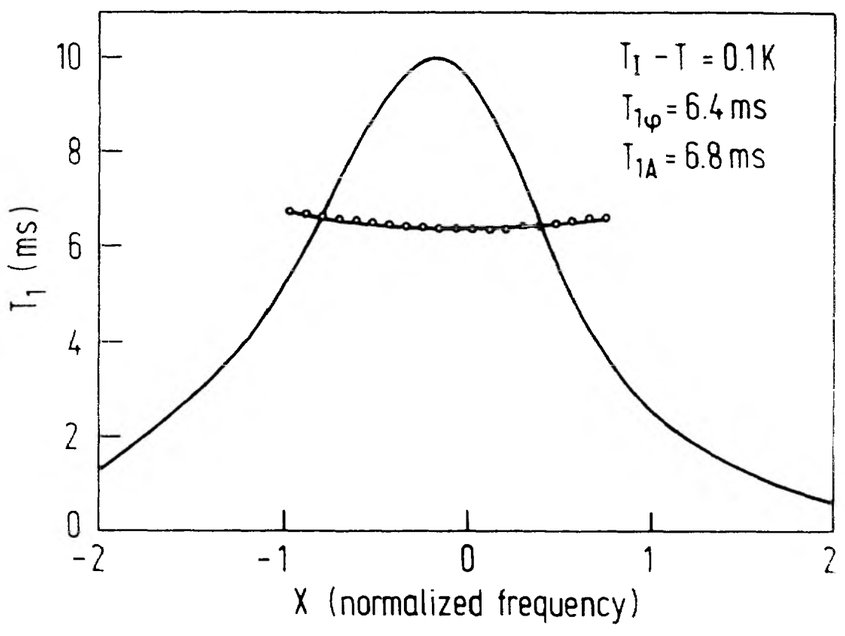

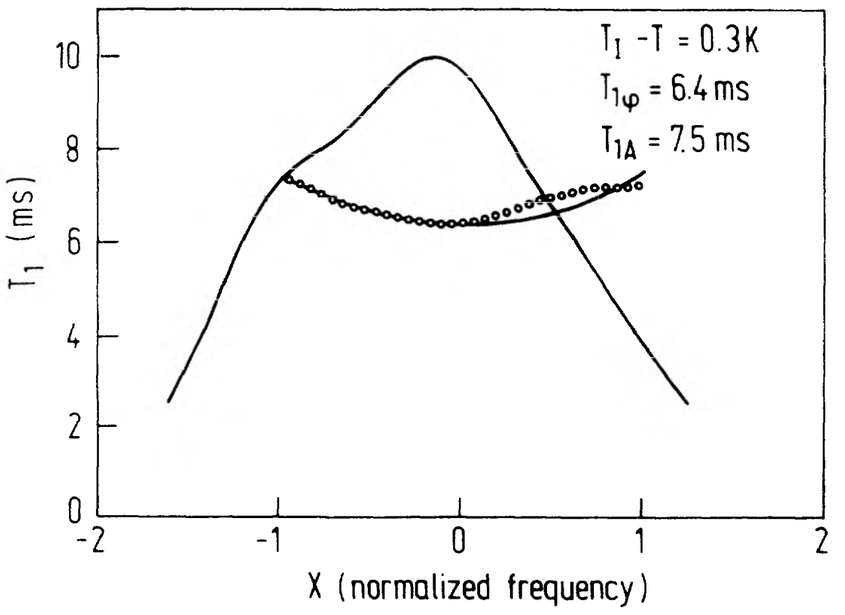

FIG. 7. Variation of the spin-lattice relaxation time T_1 over the inhomogeneous incommensurate line shape at $T_I-T=0.1$ and 0.3 K in Rb_2ZnCl_4. The orientation is the same as in Fig. 5. Circles represent measured values of T_1; fits (solid line) are made with Eq. (40).

On moving away from T_I the dynamic line shape becomes narrower, demonstrating the decreasing importance of order-parameter fluctuations. Thus the dynamic-linewidth maximum at T_I in Fig. 6 is well reproduced. Here it should be noted that, on approaching T_I from above, the increasing dynamic width is a consequence of the softening of the paraelectric soft mode. This is a doubly degenerate opticlike mode, with its frequency being described by $\omega_{SM}\propto\sqrt{T-T_I}$. Figure 9 shows the temperature variation of the parameters Ω_1, ω_{loc1}, and ω_{loc2}, determined by a comparison of experimental and theoretical line shapes. Fits of both the inhomogeneous and dynamic line shapes were made simultaneously with the same set of parameters. The parameter $\Omega_1\propto A\propto\sqrt{T_I-T}$ has been determined from the splitting of the edge singularities in a large temperature interval. Ω_1 has been then extrapolated into the critical region close to T_I, where the inhomogeneous line shapes show no edge singularities. The refined Ω_1 values after the fit procedure agreed within 10% with respect to the starting values. The temperature dependence of Ω_1 is in the general case described by $\Omega_1\propto(T_I-T)^\beta$ and the

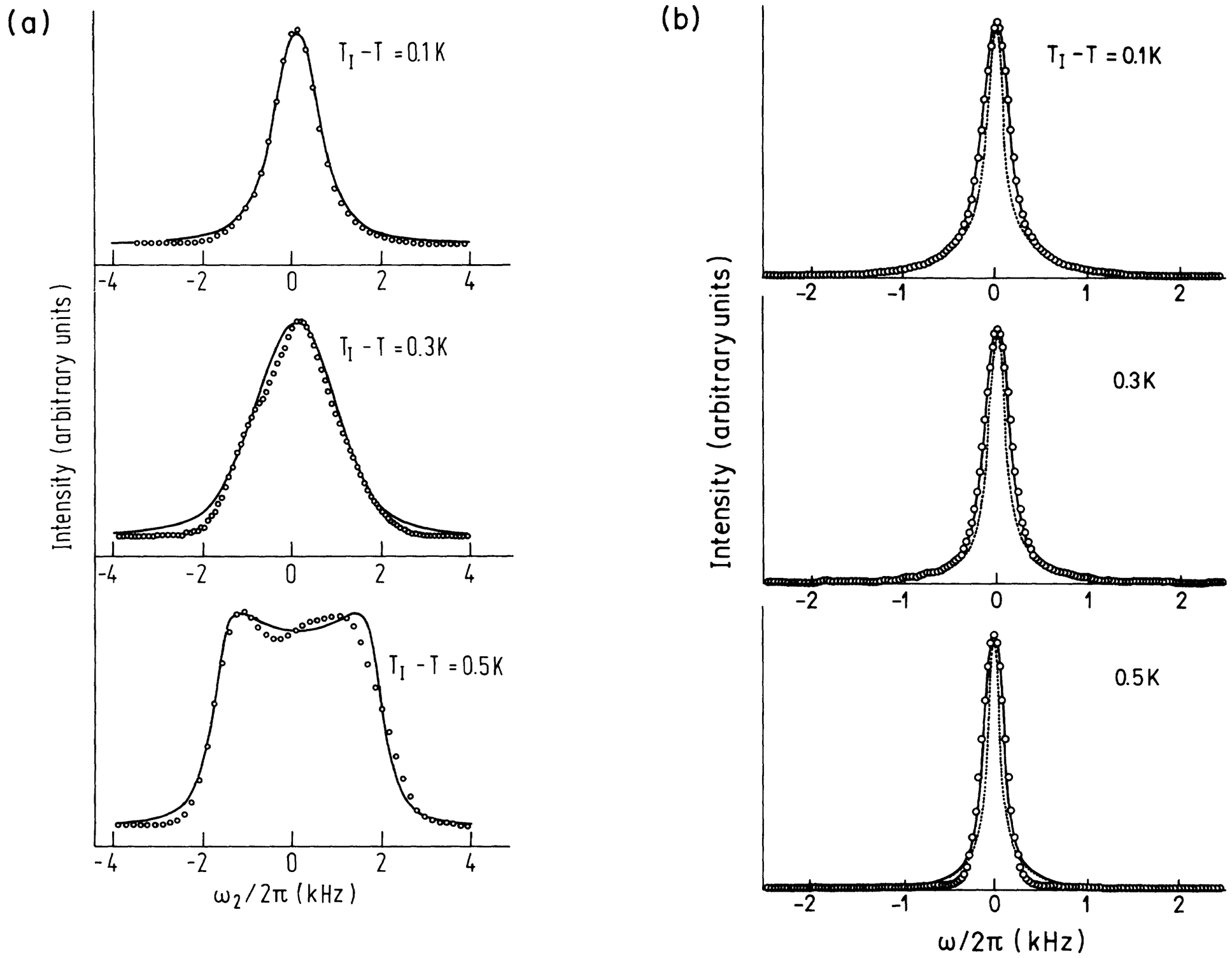

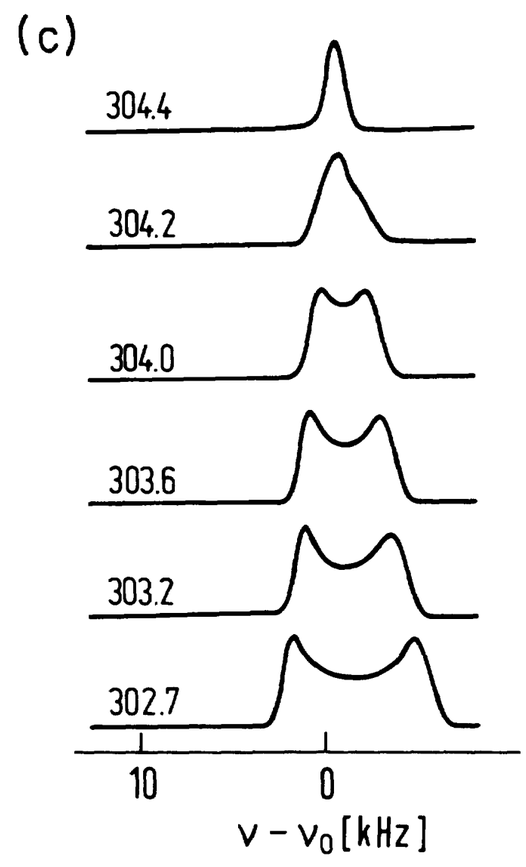

FIG. 8. (a) Experimental (open circles) and theoretical (solid line) inhomogeneous incommensurate line shapes of ^{87}Rb in Rb_2ZnCl_4 close to T_I, representing static incommensurate line shapes convoluted with the dynamic ones. Theoretical fits represent the $\omega_1=0$ cross section of the 2D spectrum [Eq. (37(b)]. The temperatures are 0.1, 0.3, and 0.5 K below T_I. (b) Experimental (open circles) and theoretical dynamic line shapes of ^{87}Rb in Rb_2ZnCl_4. The temperatures are the same as in (a). Solid lines represent the fits with Eq. (37b), corresponding to the case of a phason with a large gap, whereas dotted lines represent fits with Eq. (38), valid for a gapless phason. The large-phason-gap model calculation fits the experimental line shapes better than the gapless-phason calculation. (c) Experimental inhomogeneous line shapes in a large temperature interval. The orientation is the same as in Fig. 5.

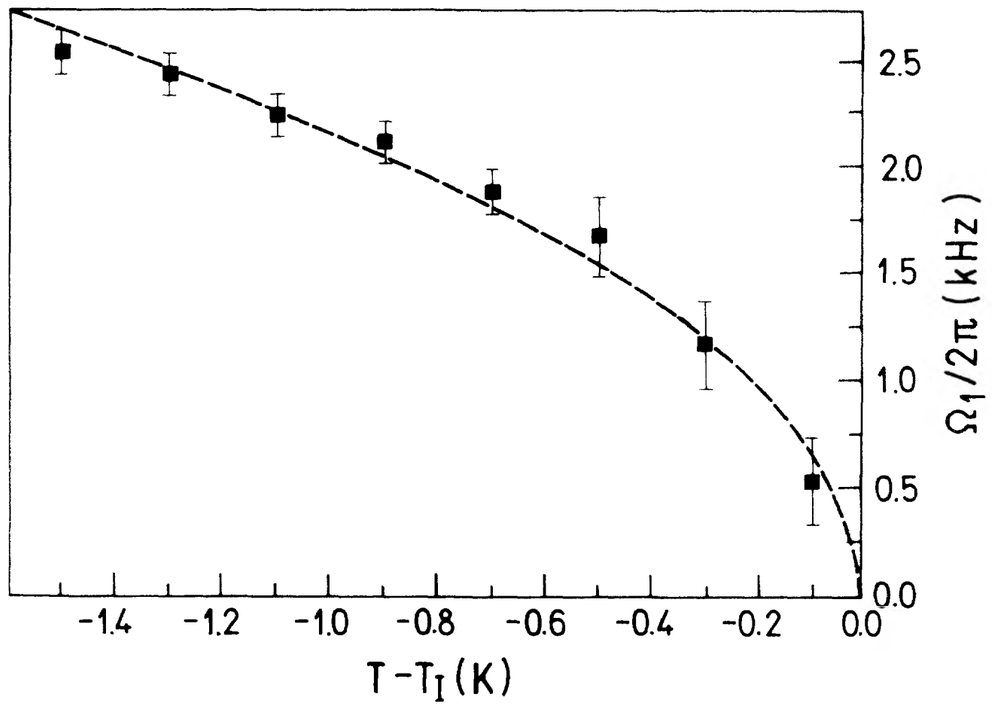

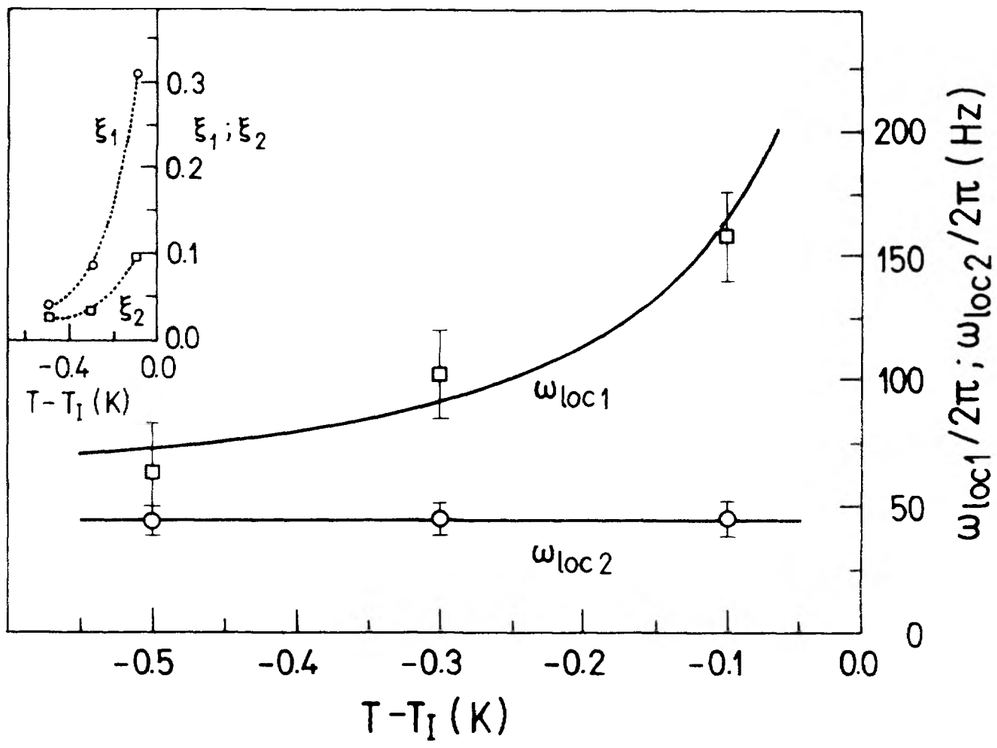

FIG. 9. Temperature dependence of the parameters $\Omega_1/2\pi$, $\omega_{loc1}/2\pi$, and $\omega_{loc2}/2\pi$ obtained by comparing experimental and theoretical inhomogeneous and dynamic line shapes. Dashed line represents a least-squares fit $\Omega_1 \propto (T_I - T)^{\beta}$ with $\beta = 0.5$. Solid lines represent fits with Eqs. (24a) and (24b). The inset shows the normalized quantities $\xi_1 = \omega_{loc1}/\Omega_1$ and $\xi_2 = \omega_{loc2}/\Omega_1$, which measure the relative sizes of the fluctuating and static parts of the order parameter. Moving away from T_I, ξ_1 and ξ_2 tend to zero.

determination of the critical exponent β strongly depends on the choice of T_I. In Rb_2ZnCl_4, NMR measurements[5,20] yielded a nonclassical value of $\beta = 0.35$. It has been shown recently that the $\beta = 0.35$ result is generally found in one-dimensionally modulated incommensurate crystals.[23] These results were obtained from NMR studies of the temperature variation of the order parameter over a large temperature interval. Our calculations are based on the Landau theory which uses the classical critical exponent $\beta = 0.5$. The fit with $\Omega_1 \propto (T_I - T)^{0.5}$ is shown as a dashed line in Fig. 9. This fit is made over a temperature interval $\Delta T = 1.6$ K close to T_I and in this interval the value $\beta = 0.5$ reproduces rather well the experimental data. In a larger temperature interval $\beta = 0.35$ has to be used for a proper fit. The fit parameter ω_{loc1} behaves as $T/\sqrt{T_I - T}$, in agreement with Eq. (24a). The solid line represents the fit with the ansatz $\omega_{loc1} = CT/\sqrt{T_I - T}$ and the constant C is found as $C = (1.1 \pm 0.1)\ \mathrm{s}^{-1}\ \mathrm{K}^{-1/2}$. ω_{loc2} is also consistent with the prediction of Eq. (24b), since it is found to decrease very weakly in a temperature interval $\Delta T = 0.5$ K below T_I. The fit (solid line) was made with the ansatz $\omega_{loc2} = DT$ and the constant D is found as $D = (0.99 \pm 0.05)\ \mathrm{s}^{-1}\ \mathrm{K}^{-1}$. The inset in Fig. 9 shows the normalized quantities

$$\xi_1 = \frac{\omega_{loc1}}{\Omega_1} \propto \frac{T}{T_I - T}$$

and

$$\xi_2 = \frac{\omega_{loc2}}{\Omega_1} \propto \frac{T}{(T_I - T)^{1/2}} ,$$

which measure the relative sizes of the fluctuating part of the order parameter with respect to the average value of the order parameter. At $T_I - T = 0.1$ K, ξ_1 amounts to 0.31 and $\xi_2 \approx 0.1$. On moving away from T_I into the incommensurate phase, ξ_1 and ξ_2 tend to zero, showing the decreasing importance of phase and amplitude fluctuations.

The values of $\xi_1 = 0.31$ and $\xi_2 = 0.1$ at $T_I - T = 0.1$ K indicate that the fluctuating and the static parts of the order parameter become of comparable size at that temperature. An interesting question arises when one considers how close to the phase transition temperature T_I the above treatment—based on the Landau theory—can be applied. It is well known that the Landau theory is applicable in the range where the order-parameter fluctuations are small compared to the static part of the order parameter. Thus approaching T_I one necessarily violates the above condition. From the normalized quantities ξ_1 and ξ_2 one can see that the parameter Ω_1—a measure of the magnitude of the static order parameter—and parameters ω_{loc1} and ω_{loc2}—measures of the fluctuating parts of the order parameter—become of comparable size 0.1 K below T_I. The above treatment thus does not apply at temperatures closer than 0.1 K to T_I.

B. ^{39}K NMR in K_2SeO_4

A similar effect of thermal fluctuations as in Rb_2ZnCl_4 has been observed also in the quadrupole-perturbed ^{39}K NMR spectra of K_2SeO_4. The ^{39}K $\frac{1}{2} \rightarrow -\frac{1}{2}$ transition has been measured at the Larmor frequency 12.6 MHz around the paraelectric-incommensurate transition temperature $T_I = 125.2$ K. The orientation of the crystal ($a \perp H_0$, $< c, H_0 = 100°$) has been chosen in such a way that the expansion of the frequency in powers of the displacements [Eq. (15a)] is linear. The ^{39}K inhomogeneous spectra are shown in Fig. 10(a) for a set of temperatures below T_I. Care has been taken to decrease the temperature gradient across the sample to less than 0.1 K by proper thermal isolation in the cryostat and by waiting at least thirty minutes before the measurement was started after the desired temperature has been reached. The inhomogeneous spectrum at $T_I - T = 0.4$ K preserves its paraelectric shape, whereas the spectra between $T_I - T = 1.6$ and 3.4 K gradually transform into the stat-

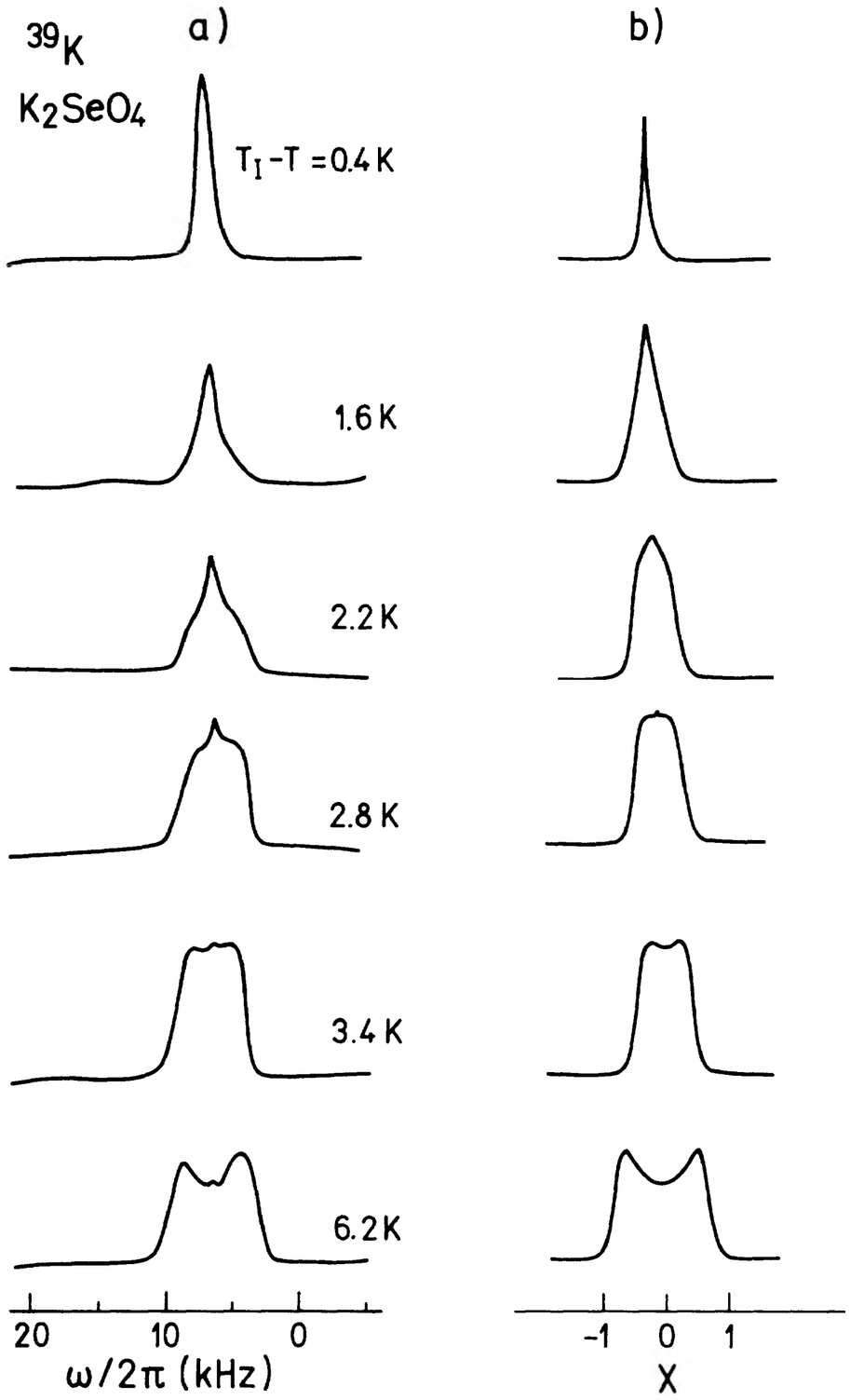

FIG. 10. (a) ^{39}K $\frac{1}{2}\rightarrow-\frac{1}{2}$ inhomogeneous NMR line shapes in K_2SeO_4 in the vicinity of $T_I=125.2$ K [$\nu_0(^{39}\text{K})=12.6$ MHz, $a\perp H_0$, $<c,H_0=100°$]. (b) Theoretical inhomogeneous line shapes in the vicinity of T_I [Eq. (28)], derived for the case of a small phason gap. The spectra are displayed on a normalized frequency scale $X=(\omega-\Omega_0)/\Omega_1$; $\xi=0.1$ and $\tilde{\xi}_2\approx B/\sqrt{(T_I-T)/T_I}$.

ic incommensurate shape. The central peak arises from the parts of the modulation wave which fluctuate fast on the linewidth scale. Another explanation for the central peak could be a distribution of T_I values due to impurities in the crystal lattice. As we are dealing with a nominally pure crystal, we believe that this alternative description is not appropriate in our case. The two possibilities cannot, however, be discriminated solely from the spectrum shape. The line shape at $T_I-T=6.2$ K corresponds to the static modulation wave, where thermal fluctuations are no longer important. Experimental line shapes have been reproduced theoretically [Fig. 10(b)] by the adiabatic inhomogeneous-line-shape formula [Eq. (28)]. As pointed out already in the Rb_2ZnCl_4 case, the inhomogeneous line shape is not sensitive enough to discriminate between different combinations of parameters $\xi_1=\omega_{\text{loc1}}/\Omega_1$ and $\xi_2=\omega_{\text{loc2}}/\Omega_1$ or $\tilde{\xi}_2=\tilde{\omega}_{\text{loc2}}/\Omega_1$. The fits with Eqs. (28) are thus qualitative only. In our fits ξ_1 assumes a small constant value 0.1 and $\tilde{\xi}_2$ is chosen in the form $\tilde{\xi}_2\approx B/\sqrt{(T_I-T)/T_I}$ with a dimensionless constant $B=5\times10^{-2}$. From Figs. 10(a) and 10(b), it can be seen that the temperature region—3 K—where thermal fluctuations affect the line shape is substantially broader in K_2SeO_4 than in Rb_2ZnCl_4.

VI. CONCLUSIONS

The obtained results show that the adiabatic incommensurate line shape is given by the Fourier transform of $\langle G\rangle=\langle G_1G_2\rangle$ and not just G_1 as tacitly assumed so far in nearly all NMR studies of incommensurate-paraelectric phase transitions. This fluctuation correction, which is similar to the Debye-Waller factor in x-ray scattering, determines the form of the NMR spectrum in the vicinity of the *N-I* transition. The 2D NMR separation technique allows for a separate observation of the static and dynamic line shapes. The latter has maximum width at T_I, thus allowing for a precise determination of T_I. This is important, since order-parameter fluctuations change the shape of the static incommensurate spectrum in such a way that the edge singularities of the static line shape disappear in a narrow temperature interval below T_I, thus masking the onset of the *I* phase.

One should note that the above fluctuation corrections are evaluated for an ideal defect-free crystal and that the NMR line shape close to T_I will be greatly influenced by impurities.

ACKNOWLEDGMENTS

This work has been supported in part by the MZT of Slovenia and the U.S. National Science Foundation under Grant No. DMR 90-24196.

[1]R. Blinc, Phys. Rep. **79**, 333 (1981).
[2]See *Incommensurate Phases in Dielectrics,* edited by R. Blinc and A. Levanyuk (North-Holland, Amsterdam, 1986), Vol. 1.
[3]J. H. Ross, Z. Wang, and P. C. Slichter, Phys. Rev. Lett. **56**, 633 (1986); B. H. Suits, S. Conturie, and C. P. Slichter, *ibid.* **45**, 194 (1980).
[4]A. Jannosy, C. Berthier, P. Slorasan, and P. Butand, Phys. Rev. **59**, 2348 (1987).
[5]R. Blinc, F. Milia, B. Topič, and S. Žumer, Phys. Rev. B **29**, 4173 (1984).
[6]R. Blinc, D. C. Ailion, P. Prelovšek, and V. Rutar, Phys. Rev. Lett. **50**, 67 (1983).
[7]M. Kogoj, S. Žumer, and R. Blinc, J. Phys. C **17**, 2415 (1984).
[8]F. Milia, R. Blinc, and S. Žumer, Solid State Commun. **50**, 1019 (1984).
[9]B. Topič, U. Haeberlen, R. Blinc, and S. Žumer, Phys. Rev. B **43**, 91 (1991).
[10]J. Emery, S. Hubert, and J. C. Fayet, J. Phys. (Paris) **46**, 2099 (1985).
[11]D. Michel, B. Muller, J. Petersson, A. Trumpert, and R. Wal-

isch, Phys. Rev. B **43**, 7505 (1991).
[12]A. M. Fajdiga, T. Apih, J. Dolinšek, R. Blinc, A. P. Levanyuk, S. A. Minyukov, and D. C. Ailion, Phys. Rev. Lett. **69**, 2721 (1992).
[13]See *Light Scattering Near Phase Transitions,* edited by H. Z. Cummings and A. P. Levanyuk (North-Holland, Amsterdam, 1983).
[14]A. Abragam, *Principles of Nuclear Magnetism* (Oxford University Press, Oxford, 1986).
[15]L. D. Landau and E. M. Lifshitz, *Statistical Physics,* 3rd ed. (Pergamon, Oxford, 1980), Part I, p. 370.
[16]R. A. Cowley and A. D. Bruce, J. Phys. C. **11**, 3577 (1978); A. D. Bruce and R. A. Cowley, *ibid.* **11**, 3609 (1978).
[17]J. Dolinšek, J. Magn. Reson. **92**, 312 (1991).
[18]R. Blinc, J. Dolinšek, P. Prelovšek, and K. Hamano, Phys. Rev. Lett. **56**, 2387 (1986).
[19]R. Blinc, J. Seliger, and S. Žumer, J. Phys. C **18**, 2313 (1985).
[20]V. Rutar, J. Seliger, B. Topič, and R. Blinc, Phys. Rev. B **24**, 2397 (1981).
[21]R. Blinc, D. C. Ailion, J. Dolinšek, and S. Žumer, Phys. Rev. Lett. **54**, 79 (1985).
[22]J. Dolinšek, T. Apih, and R. Blinc, J. Phys. Condens. Matter **4**, 7203 (1992).
[23]K.-P. Holzer, J. Petersson, D. Schüssler, R. Walisch, U. Häcker, and D. Michel, Phys. Rev. Lett. **71**, 89 (1993).